Towards the Heider balance: Cellular automaton with a global neighborhood

Malgorzata J. Krawczyk ®,* Krzysztof Kulakowski ®,† and Zdzislaw Burda ®‡

AGH University of Science and Technology, Faculty of Physics and Applied Computer Science, al. Mickiewicza 30, 30-059 Kraków, Poland

We study a simple deterministic map that leads a fully connected network to the Heider balance. The map is realized by an algorithm that updates all links synchronously in a way depending on the state of the entire network. We observe that the probability of reaching a balanced state increases with the system size N. Jammed states become less frequent for larger N. The algorithm generates also limit cycles, mostly of length 2, but also of length 3, 4, 6, 12, or 14. We give a simple argument to estimate the mean size of basins of attraction of balanced states, and we discuss the symmetries of the system including the automorphism group as well as gauge invariance of triad configurations. We argue that both symmetries play an essential role in the occurrence of cycles observed in the synchronous dynamics realized by the algorithm.

I. INTRODUCTION

In recent years, social phenomena have become an attractive field of research for scholars in statistical physics and computer science [1–4]. This interest is motivated by the spreading awareness that most of the important problems faced by mankind are created by people themselves. On the other hand, the emerging science of complexity [5] widens the list of algorithms and methods applicable to dynamic processes in social networks [1,6].

Here we focus on modeling the process of removal a cognitive dissonance [7] in social relations within a fully connected social network. During this process, the network evolves towards the so-called Heider balance, also called structural balance, where the dissonance is removed [8–10]. To the best of our knowledge, there are five different algorithms designed to model this process: two Monte Carlo algorithms [11,12] and three deterministic ones [13–16]. The first two distinguish only positive (friendly) and negative (hostile) relations. The next two are deterministic and rely on numerical solutions of differential equations for relations being represented by real numbers, which are either limited to the range $(-1, +1)$ [13] or may tend to $\pm$ infinity in a finite time [14]. The advantage of the latter approach [14] is that the equations may be solved analytically. The last method [15,16] is a deterministic synchronous cellular automaton, where the states of links are updated based on a local rule. Recently, the Monte Carlo simulations [12] have been generalized by including thermal noise [17,18] and a specific aging of the relations [19]. On the other hand, the differential equations [13] have been used to simulate asymmetric links, which mimic unreciprocated relations [20,21].

We note that most theoretical results on the Heider balance, including mathematical theorems [9], Monte Carlo simulations [11,12], and differential equations [13,14], have been obtained for fully connected networks. Two recent approaches [15,16] deal with finite neighborhoods. In Ref. [15], the rule of updating links, both deterministic and synchronous, is akin to the one used here. A deterministic and synchronous rule applied to a fully connected network is missing in the literature on the subject, and our motivation is to fill the gap. On the other hand, our results on cycles, reported below, are for small or moderate groups (N less than 30), where the presence of bilateral social relations between all individuals is not surprising [22].

In a balanced state, the relations in each triad of actors conform to the following rules [23]:

(i) A friend of my friend is my friend.

(ii) An enemy of my friend is my enemy.

(iii) A friend of my enemy is my enemy.

(iv) An enemy of my enemy is my friend.

When translated to signs of relations, the four rules allow us to distinguish balanced from imbalanced triads. In the balanced state, the product of the three signs is $+1$ in each triad. The process of reducing the dissonance in the network is equivalent to a minimization of the negative sum over all triads,

$$U = -\sum_{i<j<k}^{N} \Delta_{ijk} = -\sum_{i<j<k}^{N} s_{ij} s_{jk} s_{ki}, \quad (1)$$

where the sign $s_{ij} = \pm 1$ represents the symmetric relation between actors located in the nodes i and j of the network. One can think of U as the energy of the system. As shown in [9], when all triads are balanced, then the whole network is split into two groups, internally friendly and mutually hostile. Clearly, in such states there is no cognitive dissonance about who is friend and who is enemy.

The rest of the paper is composed as follows. In the next section, we describe the algorithm. Next (Sec. III) we

*malgorzata.krawczyk@agh.edu.pl
†kulakowski@fis.agh.edu.pl
‡zdzislaw.burda@agh.edu.pl

graphically demonstrate that for $N = 3, 4$ the system evolves immediately (in one time step) towards a balanced state, while for $N = 5$, short limit cycles, of length 2, are also possible. In Sec. IV we discuss symmetries of the system. In Sec. V we report the results on the influence of the system size on the number of transient iterations and on the probability of balanced states. Section VI is devoted to the limit cycles observed in larger systems. The paper is concluded by a discussion of results in Sec. VII and a summary in Sec. VIII.

II. ALGORITHM

In this paper, we study a discrete time evolution, which is deterministic and synchronous as for cellular automata [15], however—as in [11,13]—the basic update rule depends on the state of the entire network,

$$s_{ij}(t+1)$$

$$= \begin{cases} \text{sgn}\left(\sum_{k \neq i, j}^{N} s_{ik}(t) s_{kj}(t)\right) & \text{if} \quad \sum_{k \neq i, j}^{N} s_{ik}(t) s_{kj}(t) \neq 0, \\ s_{ij}(t) & \text{otherwise} \end{cases}$$

$$(2)$$

for all pairs $i \neq j$. The sum runs through all vertices k other than i and j. The most important difference from a typical cellular automaton is that the neighborhood of an updated edge (2) increases with the system size, hence the term "global" in the title. The difference from the Monte Carlo method is that in a single step of the algorithm, all links are updated simultaneously, based on the previous state of the system. This is a deterministic rule on a fully connected network.

The update rule (2) is equivalent to

$$s_{ij}(t+1) = \begin{cases} s_{ij}(t) & \text{if} \quad -U_{ij}(t) \equiv \sum_{k \neq i, j}^{N} \Delta_{ijk}(t) \geqslant 0, \\ -s_{ij}(t) & \text{otherwise,} \end{cases}$$

$$(3)$$

where the sum in the last equation runs over all triads sharing the edge ij. The update rule (2), or equivalently (3), can be interpreted as a majority rule according to which the sign of the edge ij adjusts to the sign of the majority of triads of which it is a part. Clearly, if the updates (3) were applied asynchronously, edge by edge, they would either leave energy (1) unchanged, $U(t+1) = U(t)$ if $U_{ij}(t) \leqslant 0$, or reduce it to

$$U(t+1) = U(t) - 2U_{ij}(t) \quad (4)$$

if $U_{ij}(t) > 0$, as a result of changing the signs of triads containing the edge ij. The update rule (3) would never increase energy. For synchronous updates this is not the case. The synchronous dynamics is much more complex, which makes it very interesting.

Let us also note that for odd N the second line in Eq. (2) may be omitted because the sum of an odd number of terms ± 1 is never zero. For even N the second line of Eq. (2) means "do nothing if there is no majority." This choice is similar to the Nash equilibrium where an actor does not change strategy if s/he cannot profit from the change [24]. This choice is also akin to the delay of updating, applied in [25] to eliminate "unstable" attractors in Boolean networks. We shall mention an alternative solution later while discussing symmetries of the system.

The rationale behind Eq. (2) is the same as in [11–16]. Namely, the relation s_{ij} of i with j is improved if the relations s_{ik} and s_{kj} are both friendly ("friend of my friend") or both hostile ("enemy of my enemy"). In two other cases ("friend of my enemy" or "enemy of my friend") the relation s_{ij} is deteriorated. Here, as in [13], this consultation of relation s_{ij} is extended over all agents k of the network. The difference with [13] is that here links are updated in one time step. The same kind of updating was applied in [15] for a local neighborhood. Our approach is complementary to the previous ones [11–16]. As we demonstrate below, the results obtained within this approach are qualitatively new. They broaden the spectrum of the types of behavior that can be observed in the evolution of social networks that are trying to achieve Heider balance.

III. SMALL SYSTEMS

For $N = 3$, there are eight distinct configurations—$(+ + +)$, $(+ + -)$, $(+ - +)$, $(- + +)$, $(- - +)$, $(- + -)$, $(+ - -)$, and $(- - -)$—that can be grouped into four distinct classes of indistinguishable unlabelled configurations, which we denote by A, A^*, B, B^*; see Fig. 1. The notation with the star superscript will become clear later. The class A has three positive links, B has two, B^* has one, and A^* has no positive links. The classes A, B^* are balanced while A^* and B are imbalanced. The class cardinality is the number of distinct labeled configurations. The cardinalities of the classes A and A^* are equal to 1, while those of B and B^* are equal to 3. The transitions between classes generated by the synchronous majority rule (2) are shown in Fig. 1. One can also list all configurations for $N = 4, 5, \ldots$. Let us first discuss in detail the case $N = 5$, which illustrates a variety of interesting effects. Later we will return to $N = 4$. The distinct unlabeled classes on the complete graph K_5 are collected in Table I. In the table, one can also see the multiplicities of the classes as
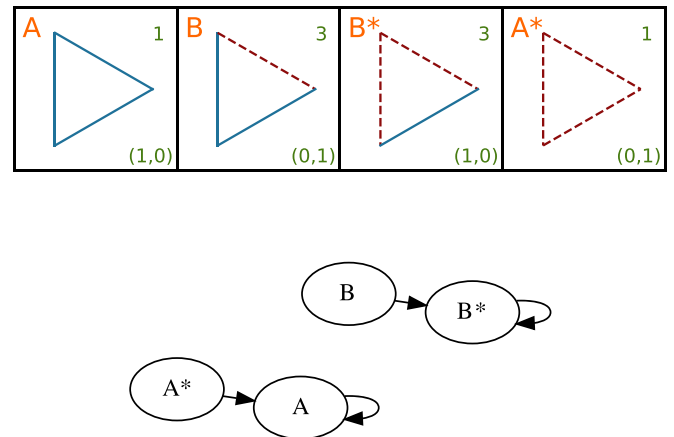
FIG. 1. Top: configuration classes for $N = 3$. The class cardinalities are given in the upper right corners of the plaquettes. In the lower right corner, in parentheses, the numbers are given of balanced and imbalanced triads. The same coding is applied below. A starred class X^* is obtained from X by swapping all signs: $+1$ to -1 and -1 to $+1$. Bottom: flow diagram representing transitions between the classes, under the synchronous update rule (2).

TABLE I. Classes of unlabeled configurations for $N = 5$, their cardinalities, and the numbers of balanced and imbalanced triads.

FIG. 2. Flow diagram representing transitions between unlabeled classes for $N = 5$, under the synchronous update rule (2).

well as the corresponding numbers of positive and negative triads, which are displayed in parentheses (Δ_+, Δ_-). It is not a complete list of configurations for $N = 5$, because we have left out the configurations that can be obtained from those shown in the table, swapping the positive and negative links. Such configurations will be denoted by a star; for instance, A^* is obtained from A so it consists only of negative edges. B^* is obtained from B and thus it has a single positive edge and nine negative ones, etc. We shall refer to starred classes as dual classes. A change of signs of all edges applied twice leaves them unchanged, then we have $A = A^{**}$. The complete graph K_5 has 10 links, and thus there are $2^{10} = 1024$ configurations. Adding cardinalities of all classes from Table I and of the corresponding dual classes, one finds that the sum is indeed equal to 1024. One should note that the classes O and Q are self-dual, that is, $O = O^*$ and $Q = Q^*$, and that the classes P and T, as well as R and S, are mutually dual $P = T^*$ and $R = S^*$. Therefore, in order to avoid double counting, the multiplicities of these classes should be counted once, as opposed to those of other classes from the table, which should be counted twice in order to take into account contributions from the class and its dual partner.

Let us now study the action of the transformation rule (2) on the classes. The result is illustrated in Fig. 2 as a flow diagram, which indicates which class is mapped into which. The diagram has seven connected components, each representing a different basin of attraction. The symbol $F2$ means a union of two classes, $F2 = F \cup F^*$, and similarly for other letters. The

double letters $PT2$ and $RS2$ are used for dual classes to underline that $T2 = P2$, and similarly $R2 = S2$. The attractors in Fig. 2 can be divided into two different types: absorbing classes, and limit cycles of order 2. There are five absorbing classes: A, I, J^*, C, and K^*, and two limit cycles of order 2: (D^*, N) and (L, M^*). Three absorbing classes are balanced: A, I, and J^*, and two are imbalanced: K^* and C. Interestingly, the absorbing classes K^* and C correspond in fact to the limit cycles of length 2, which are internal cycles between different configurations from the same class. The cycles are shown in Fig. 3. To summarize, for $N = 5$ we observe absorbing states, as well as limit cycles of length 2.

IV. SYMMETRIES

The discussed system has a high symmetry. The basic symmetry is related to the automorphism group of the complete graph, which forms the skeleton of the system. The other symmetry is related to gauge invariance of triads. Let $\{\Delta_{ijk}\}_{i<j<k}$ be the list of values of the products $\Delta_{ijk} = s_{ij}s_{jk}s_{ki}$ for all triads. The following transformation applied to all edges ij:

$$s_{ij} \rightarrow s'_{ij} = \sigma_i s_{ij} \sigma_j, \qquad (5)$$

where $\sigma_i = \pm 1$, for $i, j = 1, \ldots, N$, leaves all the products invariant,

$$\Delta'_{ijk} = s'_{ij}s'_{jk}s'_{ki} = s_{ij}s_{jk}s_{ki} = \Delta_{ijk}, \qquad (6)$$
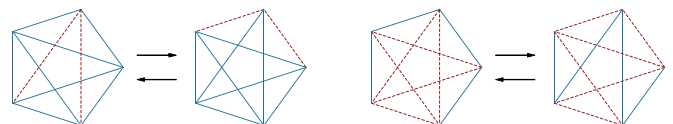
FIG. 3. Internal limit cycles within C class (left) and K^* class (right).

because each sigma is squared, yielding $\sigma_i^2 = \sigma_j^2 = \sigma_k^2 = 1$. As a consequence, the same set of values

$$\{\Delta_{ijk}\}_{i<j<k} \rightarrow \{\Delta'_{ijk}\}_{i<j<k} = \{\Delta_{ijk}\}_{i<j<k} \quad (7)$$

can be represented by distinct edge configurations. Borrowing terminology from high-energy physics, the configurations representing the same set of Δ's can be called Gribov copies [26]. Since one can have two values $\sigma_i = \pm 1$ (5) for $(N-1)$ vertices, there are 2^{N-1} Gribov copies. For one vertex (it does not matter which one), one should have only one value $\sigma_i = 1$, because as one can see from Eq. (5), when all σ's are equal to -1, all edges acquire the same values, $s'_{ij} = s_{ij}$, as in the primary configuration.

To see how it works, let us consider again the case $N = 5$. There are $2^4 = 16$ copies of each configuration. The configuration from class A can be easily copied to a configuration from class I by choosing $\sigma_i = -1$ for one vertex and $\sigma_j = 1$ for all remaining vertices $j \neq i$. In this way, all edges attached to i will change sign, yielding a configuration from the class I. If we choose $\sigma_i = \sigma_j = -1$ for two vertices, and $\sigma_k = 1$ for all remaining ones, $k \neq i, j$, we obtain a configuration from class J^*. There is one configuration in class A, five in class I, and ten in class J^*, altogether 16 copies. In a similar way, one can identify copies of any (labeled) configuration.

Coming back to the internal cycles in class C and class K^* that we discussed earlier (Fig. 5), one can easily see that the consecutive configurations are Gribov copies of one another. Actually, this is also a feature of many limit cycles that we observe for higher N.

We conclude this section by discussing yet another issue related to the symmetry of the system. As mentioned, for odd N the update rule (2) amounts to a pure majority rule

$$s_{ij}(t+1) = \text{sgn}\left(\sum_{k \neq i, j}^{N} s_{ik}(t)s_{kj}(t)\right). \quad (8)$$

The results of the action of this rule on a configuration, and a configuration obtained from it by changing globally all signs $s_{ij} \rightarrow s'_{ij} = -s_{ij}$, are identical since the additional minus signs on the right-hand side of the equation cancel. This reduces the complexity of the problem. The reduction does not apply for even N since the second line of the update rule (2) depends on individual signs. As a result, it has to be considered separately how this rule works on the configuration and its double partner. One can, however, slightly modify the update rule (2) in order to restore the symmetry with respect to the global change of all signs,

$$s_{ij}(t+1) = \text{sgn}'\left(\sum_{k \neq i, j}^{N} s_{ik}(t)s_{kj}(t)\right), \quad (9)$$

where the function sgn' is a modified sign function such that $\text{sgn}'(x) = 1$ for $x \geq 0$ and $\text{sgn}'(x) = 0$ otherwise. For large N, the number of cases when the argument is exactly equal to zero decreases, so one can expect that for large N the difference between the effects of applying the modified rule (9) and the original one (2) disappears. In Table II we list configuration classes for $N = 4$, and in Fig. 4 we illustrate the

TABLE II. Unlabeled configuration classes for $N = 4$.
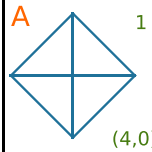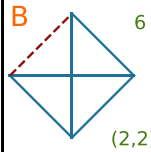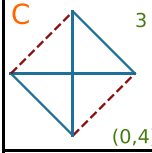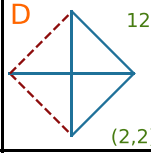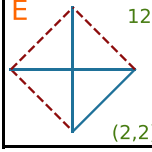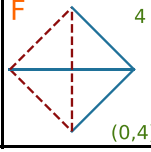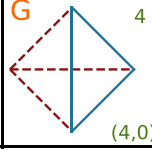
difference between the basins of attraction for the two rules. We see that some states move from one basin to another.

V. SIZE EFFECTS

The number of L links is $N(N-1)/2$ and the update (2) of each link requires the calculation of a sum of $N-2$ terms (2), so the computational complexity of a single update of the whole system is $O(N^3)$. Denote τ the number of transient updates until a fixed point or a limit cycle is reached. Numerical results on average $\tau(N)$, for a system with N nodes, are shown in Fig. 5. Let us make a rough estimate of the computational cost of the transient part of the process. $\tau(N)$ seems to increase logarithmically for large N, so the mean computational cost of reaching either a fixed point or a cycle is $O(N^3 \ln N)$. This is more than $N^{4/3}$ for the Local Triad Dynamics, $p = 1/2$ [11], where p is the probability of converting $(++-) \rightarrow (+++)$. On the other hand, this is much less than the cost of solving numerically $N^2/2$ equations [13].

We have also evaluated the fraction B of balanced states among the steady states. The results are shown in Fig. 6. In general, the fraction B increases with N. This result is similar to the result [11] that the probability of imbalanced steady (jammed) states decreases with the system size. The values of B follow different patterns for odd and even values of N.
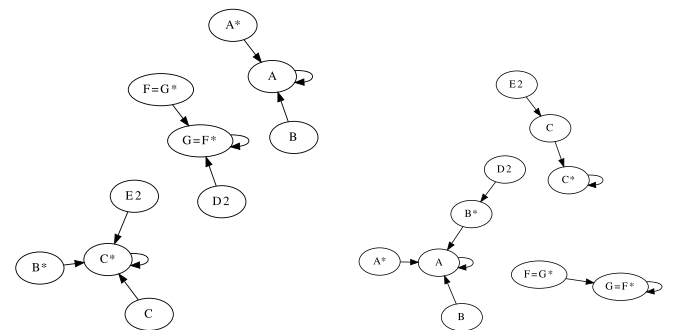
FIG. 4. Left: flow diagram for the update rule (3). Right: flow diagram for the update rule (9).
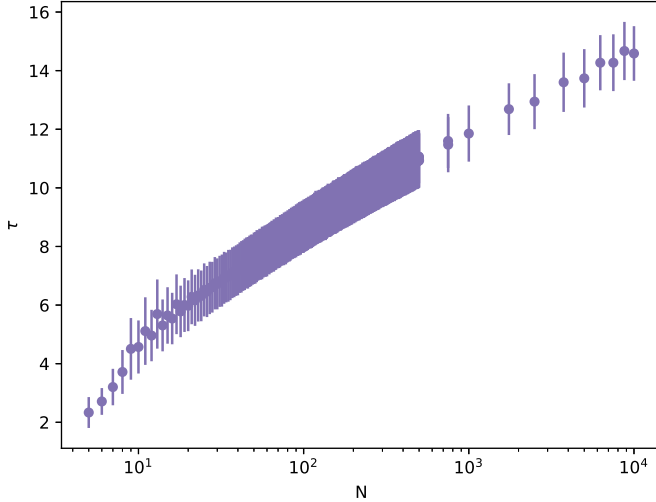
FIG. 5. The average number, $\tau = \tau(N)$, of transient time steps vs the systems size, N. The mean $\tau(N)$ was calculated from 10^4 process repetitions for $N < 30$, 5×10^3—for $30 < N < 10^3$, 400—for larger N.

The even-odd effect comes from the second line of Eq. (2), which for even N prevents some changes towards the balance.

While we do not have a detailed understanding of the dependence of B on the system size, some hints can be drawn from analogous data shown in [11], Fig. 4. Each state that is qualified as jammed in the Constrained Triad Dynamics [11], where the updates are sequential, is jammed also in our case. On the contrary, the synchronous update dynamics applied in our study classifies also other states either as jammed or as belonging to limit cycles. In [11], there are no jammed states at all until $N = 9$; therefore, the probability of such states rises from zero to a local maximum at $N = 9$ and then decreases gradually for larger systems in a way that is dependent on the initial number of positive links. In our case, the same probability J (see Table III) rises from zero to a maximum at $N = 6$ and later decreases. The increase of the fraction B
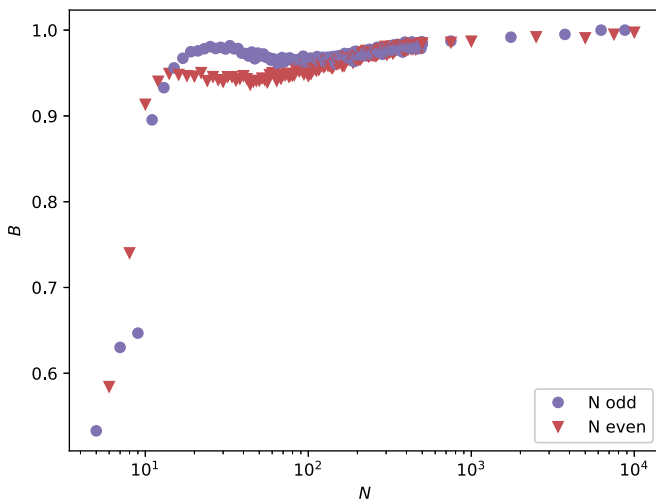
FIG. 6. The fraction, B, of balanced states vs the system size, N. The results for odd N's are plotted with circles, while for even N's they are plotted with triangles. The statistics is the same as in Fig. 5.

TABLE III. The fraction of balanced states B, of jammed states J, and of limit cycles C, as dependent on the system size N. The statistics is the same as in Fig. 5.

N	B	J	C
5	0.5329	0.0	0.4671
6	0.5844	0.2385	0.1771
7	0.6302	0.0	0.3698
8	0.7403	0.0412	0.2185
9	0.6468	0.0150	0.3382
10	0.9135	0.0378	0.0487
11	0.8954	0.0030	0.1016
12	0.9403	0.0335	0.0262
13	0.9329	0.0011	0.0660
14	0.9494	0.0359	0.0147
15	0.9560	0.0008	0.0432
16	0.9482	0.0397	0.0121
17	0.9672	0.0009	0.0319
18	0.9468	0.0424	0.0108
19	0.9748	0.0019	0.0233
20	0.9462	0.0448	0.0090
21	0.9758	0.0029	0.0213
22	0.9504	0.0417	0.0079
23	0.9783	0.0045	0.0172
24	0.9410	0.0500	0.0090
25	0.9808	0.0065	0.0127
26	0.9457	0.0478	0.0065
27	0.9786	0.0094	0.0120
28	0.9421	0.0523	0.0056
29	0.9800	0.0097	0.0103
30	0.9398	0.0544	0.0058
50	0.9412	0.0552	0.0036
75	0.9670	0.0302	0.0028
100	0.9466	0.0508	0.0026

of balanced states is additionally moderated by the fraction C of limit cycles, which are absent in the case of sequential dynamics [11].

As we mentioned above, the fraction B of balanced states is different for odd and even values of N because for even N, the right-hand side of Eq. (2) is sometimes equal to zero. We note that as N increases, the probability of such configurations decreases, and the results on B for even and odd values of N approach the same asymptotic curve.

VI. LIMIT CYCLES

Obviously a limit cycle cannot be balanced because balanced states are absorbing, as follows from (2). For a Monte Carlo evolution there are no limit cycles, as the system is driven either to a balance or a jammed state [11,12]. Here we observe both jammed states and limit cycles. An example of a limit cycle is shown in Fig. 7. In Table III, detailed statistics of states leading to different attractors is presented. From these data, the following new observations can be deduced:

(i) The increase of the fraction, B, of balanced states with N for $14 < N < 100$ is slow and it is visible only for larger N, as shown in Fig. 6. In this smaller range of N, B is slightly larger for odd values of N.
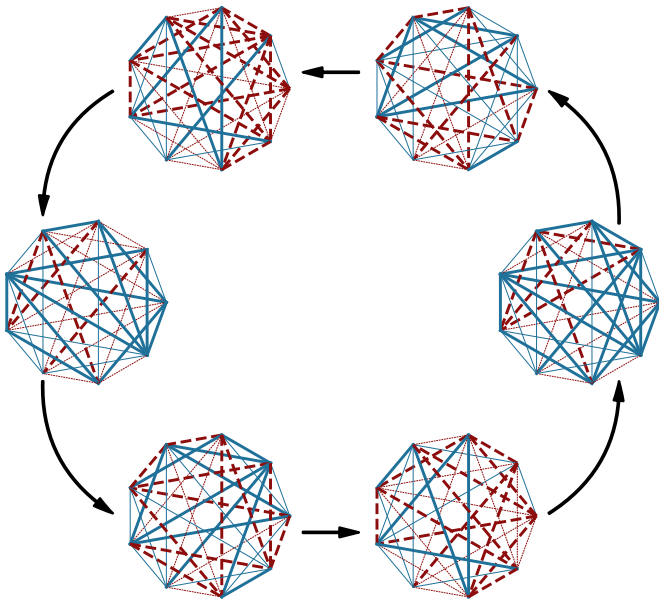
FIG. 7. An example of a nontrivial limit cycle. In the figure we show a cycle of length 6 for $N = 9$. The edges that have changed in the last step are drawn with a thick line, and those that have not are changed with a thin line.

(ii) On the contrary, the fraction J of jammed states is larger for even values of N.

(iii) The fraction C of limit cycles decreases with N, so it is much easier to encounter a limit cycle for small systems. The number of limit cycles seems to be slightly larger for odd values of N than for comparable even values.

For $N = 5$ and larger, we observe limit cycles of length $L_c = 2$. For $N = 7$–11 also limit cycles of length 3 occur. Further, $L_c = 4$ has been encountered for $N = 9$, 10, 11, and 13, $L_c = 6$ for $N = 9$ and 11, and $L_c = 12$ for $N = 9$. The longest limit cycles we observed were of length 14 for $N = 11$ (Tables IV and V). To get more insight into the case $N = 9$, we enumerated all initial configurations and calculated the numbers of initial conditions which lead to cycles of a given length. All initial 2^{36} link configurations have been browsed. The results are given in Table IV. Clearly, the sums of numbers c_k in each row are equal to $36!/N_1!/(36 - N_1)!$, where N_1 is the number of positive links (and $N_{-1} = L - N_1$ is the number of negative links).

The cycle distribution does not change when we interchange N_1 and N_{-1}. This is a demonstration of the global symmetry of Eq. (2) under the change of signs of all links. The symmetry holds only for odd values of N. For even values, the second line of Eq. (2) breaks the symmetry, as discussed in Sec. III.

We checked that for $N = 9$ even for long cycles, the energy U either remains constant during a cycle or takes at most two values. For $L_c = 2$, these values that appear alternately are -24 and -6; the others are -52, -22, -20, -18, and -2. For $L_c = 3$, the energy remains constant during each cycle, and its value is -14, -6, or $+8$. For $L_c = 4$, a possible cycle of U is -12, -12, $+4$, $+4$; the energy fixed points are -12, -10, or -4. For $L_c = 6$ either $U = +2$ or a cycle appears: 0, 0, 0, $+2$, $+2$, $+2$. Finally, for $L_c = 12$ we get only a fixed point $U = -6$.

To complete the overall picture, we determined the cycles lengths also for $N = 7$, 11 with better statistics. For $N = 7$ we browsed all initial configurations. For $N = 7$ the longest cycle

TABLE IV. The numbers c_k of initial states that lead to cycles of given length k for $N = 9$. In two first columns on the left, the numbers of positive N_1 and negative N_{-1} links in the initial states are given. In the two last rows, the sums and fractions of all lengths of the limit cycles are given, including those for $N_1 > N_{-1}$, not shown here.

N_1	N_{-1}	c_1	c_2	c_3	c_4	c_6	c_{12}
0	36	1					
1	35	36					
2	34	630					
3	33	7140					
4	32	58275	630				
5	31	351792	25200				
6	30	1713432	234360				
7	29	7229700	1105020	12960			
8	28	23731605	6311655	194400	22680		
9	27	68512360	23499000	1360800	362880	272160	136080
10	26	163379286	77290290	6259680	3084480	3265920	907200
11	25	405524196	164254860	20049120	3447360	3810240	3719520
12	24	798887565	365041215	49260960	14719320	20321280	3447360
13	23	1548952020	634738860	80831520	11793600	17781120	16692480
14	22	2467970100	1093051260	140019840	39009600	46811520	9434880
15	21	3798647280	1507217040	160885440	33203520	37195200	30754080
16	20	4770389610	2096265780	240226560	79606800	100154880	21228480
17	19	5850581940	2318217300	274337280	44089920	57062880	53207280
18	18	5862580080	2640716820	326894400	98703360	123379200	22861440
Σ		45674454016	19215221760	2273771520	557383680	696729600	301916160
%		66.5	28.0	3.3	0.8	1.0	0.4

TABLE V. The fractions of cycle length for $N = 11$. The number of encountered cycles of length 14 is 11 172 out of 10^{10} sampled configurations.

L_c	fraction
1	0.8987022
2	0.1007681
3	0.0002326
4	0.0001544
6	0.0001416
14	0.0000011

has length $L_c = 3$. These cycles of length 3 occur in 368 640 out of 2^{21} cases (giving an approximate frequency 0.176). For $N = 11$ we sampled uniformly 10^{10} initial states out of all $2^{55} \approx 0.36 \times 10^{17}$ states, so the minimal frequency that can be detected is $O(10^{-7})$. The longest cycles recorded are of $L_c = 14$. The frequencies of different values of L_c are given in Table V. While analyzing the table, one has to remember that some objects that are less frequent than the limiting frequency $O(10^{-7})$ may not show up in the sample statistics.

It is clear that the frequency of limit cycles decreases with the system size N. Yet, as shown in Table III, cycles can appear quite frequently for small systems, for N between 5 and 11. In sociological terms, a cycle is a permanent oscillation of mutual relations, driven by the tendency to reduce cognitive dissonance about friendship and enmity. Although such social cycles are always subject to external perturbations, some variations of the relations could be repeated day by day for a relatively long time.

VII. DISCUSSION

Our result that the fraction B of balanced states increases with N is consistent with the results of [11,12] obtained with the stochastic algorithm of Local Triad Dynamics. We note that the number of balanced states increases with N as 2^{N-1}, which is much slower than the number of all states: $2^{N(N-1)/2}$. The increase of B with N indicates that the common size of the basins of attraction of balanced states increases with the system size. By definition, basins of attraction of different states do not overlap. Then we can evaluate an average size S_B of the basin of attraction of a balanced state. As we read from Table III and Fig. 6, the probability of the balanced state at the end of evolution increases with N. This probability can be evaluated as $2^{N-1}S_B/2^{N(N-1)/2}$. This means that S_B increases with N roughly as $2^{N^2/2}$. Some evaluations [27] indicate that all balanced states are equally probable. If this is the case, S_B is just the size of the basin of attraction of each balanced state, and not only the average.

The number 2^{N-1} of balanced configurations is just the number of Gribov copies of the configuration having all balanced triads. But as we discussed in the section on symmetries, in fact any triad configuration has 2^{N-1} copies. The question is whether one can invent an algorithm that would avoid this 2^{N-1}-fold degeneracy of triad configurations. The answer is affirmative. One can use a gauge fixing procedure that exploits the invariance (5) to fix signs of $(N-1)$ edges on a spanning tree. Given a spanning tree and a configuration

of signs $\{s_{ij}\}$, one can use the invariance (5) to choose σ_i's to set $s'_{ij} = \sigma_i s_{ij} \sigma_j = 1$ for every edge of the spanning tree. One can do this iteratively, edge by edge of the tree: first by choosing σ's at the end points of the first edge to set the edge sign to 1, then by choosing σ at the remaining end point of a neighboring edge, and repeating it for the next edge incident with either of the first two, etc. One can easily convince oneself that the freedom in choosing σ_i's allows one to do fix signs $s'_{ij} = 1$ on any acyclic subgraph. The spanning tree is just an acyclic connected subgraph containing all N vertices. It has $(N-1)$ edges. As a spanning tree we can choose a vertex with all $(N-1)$ edges attached to it and fix the signs of all these edges to 1. The remaining edges form a complete graph K_{N-1}. The idea is now to update only edges on this K_{N-1} subgraph using the original update rule (2), and leave the signs of the $(N-1)$ edges on the spanning tree. In this way, we reduce the problem from K_N to K_{N-1}. The price to pay is that this update scheme breaks the symmetry of the original graph, while the emergence of cycles that we discussed seems to be deeply rooted in this symmetry.

Let us now argue why the probability of reaching the fully balanced state asymptotically tends to unity for $N \to \infty$ for synchronous dynamics (2). We shall do this by comparing the synchronous dynamics to the asynchronous one, which we shall try to understand first. As discussed, energy never increases when updates (3) are done asynchronously. It is still not understood what ensures that the process of energy lowering will not stop before the energy minimum is reached. It might stop if there were no links in the system for which $U_{ij} > 0$ (3). One can show, however, that there is at least one link ij such that $U_{ij} > 0$, as long as energy U is greater than the minimal one. Thus the asynchronous algorithm will not stop until the energy minimum, and thus the full balance, is reached. For the synchronous updates (2), energy may increase. Let us suppose that $U_{ij}(t) > 0$ and $U_{kl}(t) > 0$ for two disjoint edges ij and kl, and $U_{ab}(t) \leqslant 0$ for all other edges ab. Then the net change of energy is $U(t + 1) = U(t) - 2U_{ij}(t) - 2U_{kl}(t)$, which is as if one updated edges asynchronously one after another, Eq. (4). The situation gets complicated, however, when $U_{ij}(t) > 0$ and $U_{jk}(t) > 0$ for two incident edges ij and jk, and $U_{ab}(t) \leqslant 0$ for all others ab. In this case, $U(t + 1) = U(t) - 2U_{ij}(t) - 2U_{jk}(t) + 2\Delta_{ijk}(t)$, because the triad $\Delta_{ijk}(t)$ is common for sets of triads to which the edges ij and jk belong. We see that the result of acting synchronously on edges having overlapping triads may increase energy as compared to the asynchronous update. In a more general situation, when there are more than two edges for which $U_{ij} > 0$, the energy of the system may increase, $U(t + 1) > U(t)$, after the update. This effect is frequently seen for small systems and it disappears when the system size gets bigger. When the system size increases, the system gets diluted in the sense that two incident edges have one common triad while each of them belongs to $N - 2$ triads. Thus the interference from the overlap is $1/(N-2)$ compared to the asynchronous update and disappears for $N \to \infty$. Roughly speaking, for larger systems one can expect that the synchronous update scheme behaves like the asynchronous one for a majority of configurations. For some configurations, however, due to their symmetry, limit cycles are observed. They are sort of symmetry traps. The simplest example is a configuration being a generalization

of the configuration C that we discussed for $N = 5$. More generally, for $N = 2n + 1$, such a configuration consists of all positive links except n negative links, which are incident with a vertex. One can easily see that the synchronous update (2) will map this configuration into a configuration that also has only n negative links incident with the vertex. They are complementary to those that were negative in the original configuration. The two configurations form a limit cycle. We can give more explicit examples, but as of yet we do not have a straightforward way of identifying configurations that lead to most of the observed limit cycles, especially those of length 12 or 14. We find it a very challenging problem.

The difference between the results for even and odd values of N, shown in Table III, can be attributed to the fact that for even N the function sign( ) in Eq. (2) can return zero. According to the update rule (2), in such a case the value of the link in question remains unchanged. As a consequence, the evolution towards the balance is stopped for some even values of N; hence B is smaller and J is larger there. However, for larger values of N the zero value of the right-hand side of Eq. (2) is less likely, and therefore the effect is weaker.

As shown in Sec. V, the length L_c of limit cycles increases around $N = 9$, which makes this particular size specific. To interpret the effect, let us recall that $N = 9$ has been identified in [11,12] as the minimal size of the network where jammed states exist. In other words, $N = 9$ is a boundary value between two regimes, where jammed states appear and do not appear. It is interesting that this boundary is visible in two different settings: the stochastic evolution towards the balance in [11,12], and the deterministic evolution modeled by Eq. (2). Perhaps long limit cycles can be interpreted as markers of shallow minima of a work function also in other deterministic models.

The global coupling of links in our approach makes it similar to the N-K Kauffman model of genetic systems, with the highly correlated case $K = N - 1$ [28]. In particular, the number of local optima is large (here 2^{N-1}), and the length of adaptive walks to optima increases as a logarithmic function of N. However, what evolves here is not the nodes but the links, which means that the counterpart of N in the Kauffman model is the number of links, which is $L \approx N^2/2$. The evolution of a given link is determined by the state of $2(N - 2) \approx \sqrt{8L}$ other links, which increases slower than the dimensionality L. This indicates that the similarity with the case $K = N - 1$ is incomplete.

Two comments may be added, one from a sociological perspective and one from a computational point of view. Our results, obtained within the cellular automata formalism, show that the process of removing cognitive dissonance in small groups might be counterproductive. In particular, the number of imbalanced triads can be larger than the number of balanced ones; this is the case of positive values of energy U. As the real process appears in conditions of imperfect information and a dynamically varying situation [29–32], the importance of a time sequence cannot be neglected. Yet this effect seems to lose its relevance for larger groups.

From a computational or a dynamic point of view, the results indicate that the system of size close to $N = 9$ exhibits specific properties, namely one can observe relatively frequently nontrivial, long limit cycles. This seems to be the result of a compromise between two effects. On the one hand, the length of the limit cycles increases with the system size. On the other hand, the frequency of cycles, relative to balanced states, decreases with the system size. The two effects meet for N close to 9 in the sense that for systems of the size in this range there are already longer cycles, and on the other hand they are sufficiently abundant to be observed when states are sampled randomly. We are not aware of any report on this effect in the literature. We note that the rules on friends and enemies, mentioned in the Introduction, are equivalent to negative XOR in Boolean Logic. Perhaps similar results could be obtained also for other Boolean functions. In such a case, systems of characteristic size should find application as loosely connected components of more complex entities.

VIII. CONCLUSIONS

In this paper, we considered a process of reduction of cognitive resonance, based on synchronous updates of bilateral relations between all actors forming a group. The model is realized by a deterministic update rule on a fully connected network. The new and most interesting result is the appearance of long limit cycles. Cycles of length 2 were observed already in a related model [15] when using a cellular automaton with a local neighborhood, but in the model studied in this paper the length of detected cycles is found to reach 12 for a network for $N = 9$ nodes, and 14 for $N = 11$. The frequency of long cycles strongly decreases with the system size, so the search of cycles, which is based on exhaustive browsing of all configurations, becomes very computationally expensive as N increases. It would be interesting to find an analytic argument on the probability of limit cycles for any N. The recently reported discovery [33] of a relation between the Heider balance and the Kuramoto synchronization increases the list of potential applications of the cycles.

[1] C. Castellano, S. Fortunato, and V. Loreto, Statistical physics of social dynamics, Rev. Mod. Phys. **81**, 591 (2009).

[2] P. Sen and B. K. Chakrabarti, *Sociophysics. An Introduction* (Oxford University Press, Oxford, 2013).

[3] F. Schweitzer, Sociophysics, Phys. Today **71**(2), 40 (2018).

[4] S. Galam, *Sociophysics. A Physicist's Modeling of Psychopolitical Phenomena* (Springer-Verlag, New York, 2012).

[5] S. Thurner, R. Hanel, and P. Klimek, *Introduction to the Theory of Complex Systems* (Oxford University Press, Oxford, 2018).

[6] S. P. Borgatti, M. G. Everett, and J. C. Johnson, *Analyzing Social Networks* (Sage, Los Angeles, 2013).

[7] L. Festinger, *A Theory of Cognitive Dissonance* (Stanford University Press, Stanford, 1957).

[8] F. Heider, Attitudes and cognitive organization, J. Psych. **21**, 107 (1946).

[9] D. Cartwright and F. Harary, Structural balance: A generalization of Heider's theory, Psych. Rev. **63**, 277 (1956).

[10] P. Bonacich and P. Lu, *Introduction to Mathematical Sociology* (Princeton University Press, Princeton, NJ, 2012).

[11] T. Antal, P. L. Krapivsky, and S. Redner, Dynamics of social balance on networks, Phys. Rev. E **72**, 036121 (2005).

[12] T. Antal, P. Krapivsky, and S. Redner, Social balance on networks: The dynamics of friendship and enmity, Physica D **224**, 130 (2006).

[13] K. Kułakowski, P. Gawroński, and P. Gronek, The Heider balance: A continuous approach, Int. J. Mod. Phys. C **16**, 707 (2005).

[14] S. A. Marvel, J. Kleinberg, R. D. Kleinberg, and S. H. Strogatz, Continuous-time model of structural balance, Proc. Natl. Acad. Sci. (USA) **108**, 1771 (2011).

[15] K. Malarz, M. Wołoszyn, and K. Kułakowski, Towards the Heider balance with a cellular automaton, Physica D **411**, 132556 (2020).

[16] K. Malarz and K. Kułakowski, Heider balance of a chain of actors as dependent on the interaction range and a thermal noise, Physica A **567**, 125640 (2021).

[17] F. Rabbani, A. H. Shirazi, and G. R. Jafari, Mean-field solution of structural balance dynamics in nonzero temperature, Phys. Rev. E **99**, 062302 (2019).

[18] R. Shojaei, P. Manshour, and A. Montakhab, Phase transition in a network model of social balance with Glauber dynamics, Phys. Rev. E **100**, 022303 (2019).

[19] S. Arabzadeh, M. Sherafati, F. Atyabi, G. R. Jafari, and K. Kułakowski, Lifetime of links influences the evolution towards structural balance, Physica A **567**, 125689 (2021).

[20] F. Hassanibesheli, L. Hedayatifar, P. Gawroński, M. Stojkow, D. Żuchowska-Skiba, and K. Kułakowski, Gain and loss of esteem, direct reciprocity and Heider balance, Physica A **468**, 334 (2017).

[21] M. J. Krawczyk, M. Wołoszyn, P. Gronek, K. Kułakowski, and J. Mucha, The Heider balance and the looking-glass self: modelling dynamics of social relations, Sci. Rep. **9**, 11202 (2019).

[22] R. I. M. Dunbar, Neocortex size as a constraint on group size in primates, J. Human Evol. **22**, 469 (1992).

[23] E. Aronson and V. Cope, My enemy's enemy is my friend, J. Personality Social Psych. **8**, 8 (1968).

[24] P. Straffin, *Game Theory and Strategy* (Mathematics Association of America, Washington, D.C., 1993).

[25] K. Klemm and S. Bornholdt, Stable and unstable attractors in Boolean networks, Phys. Rev. E **72**, 055101(R) (2005).

[26] V. N. Gribov, Quantization of non-Abelian gauge theories, Nucl. Phys. B **139**, 1 (1978).

[27] M. J. Krawczyk, S. Kałużny, and K. Kułakowski, A small chance of paradise—equivalence of balanced states, Europhys. Lett. **118**, 58005 (2017).

[28] S. A. Kauffman, *The Origins of Order. Self-Organization and Selection in Evolution* (Oxford University Press, New York, 1993).

[29] J. W. Brehm, Increasing cognitive dissonance by a fait accompli, J. Abnormal Social Psych. **58**, 379 (1959).

[30] J. D. Jecker, Conflict and dissonance: a time of decision, in *Theories of Cognitive Consistency: A Sourcebook*, edited by R. P. Abelson, E. Aronson, W. J. McGuire, Th. M. Newcomb, M. J. Rosenberg, and P. H. Tannenbaum (Rand McNally, Chicago, 1968).

[31] J. E. Russo, M. G. Meloy, and V. H. Medvec, Predecisional distortion of product information, J. Marketing Res. **35**, 438 (1998).

[32] Y. H. Liang, Reading to make a decision or to reduce cognitive dissonance? The effect of selecting and reading online reviews from a post-decision context, Comput. Human Behavior **64**, 463 (2016).

[33] M. T. Schaub, N. O'Clery, Y. N. Bileh, J.-C. Delvenne, R. Lambiotte, and M. Barahona, Graph partitions and cluster synchronization in networks of oscillators, Chaos **26**, 094821 (2016).